A bioengineered peripheral nerve construct using aligned peptide amphiphile nanofibers

Andrew Li[#a], **Akishige Hokugo**[#a], **Anisa Yalom**[a], **Eric J. Berns**[b,c], **Nicholas Stephanopoulos**[b], **Mark T. McClendon**[d], **Luis A. Segovia**[a], **Igor Spigelman**[e], **Samuel I. Stupp**[b,f,g,h], and **Reza Jarrahy**[a,*]

[a]Division of Plastic and Reconstructive Surgery, Department of Surgery, David Geffen School of Medicine at UCLA, Los Angeles CA, 90095-6960, USA

[b]Institute for Bionanotechnology in Medicine, Northwestern University, Evanston, IL, 60208, USA

[c]Department of Biomedical Engineering, Northwestern University, Evanston, IL, 60208, USA

[d]Department of Chemical and Biological Engineering, Northwestern University, Evanston, IL 60208, USA

[e]Division of Oral Biology and Medicine, UCLA School of Dentistry, Los Angeles CA, 90095 USA

[f]Department of Materials Science and Engineering, Northwestern University, Evanston, IL, 60208, USA

[g]Department of Chemistry, Northwestern University, Evanston, IL, 60208, USA

[h]Department of Medicine, Northwestern University, Evanston, IL, 60208, USA

[#] These authors contributed equally to this work.

Abstract

Peripheral nerve injuries can result in lifelong disability. Primary coaptation is the treatment of choice when the gap between transected nerve ends is short. Long nerve gaps seen in more complex injuries often require autologous nerve grafts or nerve conduits implemented into the repair. Nerve grafts, however, cause morbidity and functional loss at donor sites, which are limited in number. Nerve conduits, in turn, lack an internal scaffold to support and guide axonal regeneration, resulting in decreased efficacy over longer nerve gap lengths. By comparison, peptide amphiphiles (PAs) are molecules that can self-assemble into nanofibers, which can be aligned to mimic the native architecture of peripheral nerve. As such, they represent a potential substrate for use in a bioengineered nerve graft substitute. To examine this, we cultured Schwann cells with bioactive PAs (RGDS-PA, IKVAV-PA) to determine their ability to attach to and

*Corresponding author: Reza Jarrahy, M.D., Division of Plastic and Reconstructive Surgery, Department of Surgery, David Geffen School of Medicine at UCLA, Address: 200 UCLA Medical Plaza, Suite 465 Los Angeles, CA 90095-6960, Phone: 310-825-0065, Fax: 310-794-7933, rjarrahy@mednet.ucla.edu.

proliferate within the biomaterial. Next, we devised a PA construct for use in a peripheral nerve critical sized defect model. Rat sciatic nerve defects were created and reconstructed with autologous nerve, PLGA conduits filled with various forms of aligned PAs, or left unrepaired. Motor and sensory recovery were determined and compared among groups. Our results demonstrate that Schwann cells are able to adhere to and proliferate in aligned PA gels, with greater efficacy in bioactive PAs compared to the backbone-PA alone. *In vivo* testing revealed recovery of motor and sensory function in animals treated with conduit/PA constructs comparable to animals treated with autologous nerve grafts. Functional recovery in conduit/PA and autologous graft groups was significantly faster than in animals treated with empty PLGA conduits. Histological examinations also demonstrated increased axonal and Schwann cell regeneration within the reconstructed nerve gap in animals treated with conduit/PA constructs. These results indicate that PA nanofibers may represent a promising biomaterial for use in bioengineered peripheral nerve repair.

Keywords

Self assembly; Peptide amphiphile; Alignment; Peripheral nerve repair; Nerve conduit; Nerve regeneration; Nanofiber

1. Introduction

It is estimated that at least 200,000 peripheral nerve repairs are performed annually in the United States [1]. Traumatic peripheral nerve injuries represent a particular challenge for reconstructive surgeons due to their strong association with long-term disability and poor functional outcomes. For example, only 7% of patients who sustain a gunshot wound to an extremity with a resultant peripheral nerve injury attain normal limb function, compared to 39% of patients who achieve functional recovery in the setting of a gunshot-induced extremity injury without nerve involvement [2]. This poor prognosis is due to the principle of Wallerian degeneration, whereby the nerve segment distal to the site of injury becomes dysfunctional, which in turn leads to atrophy and malfunction of the end organ supplied by the nerve.

Various techniques for nerve repair exist. Direct neurorrhaphy (end-to-end repair) of a transected nerve is an effective means of repair when there is no gap between the cut nerve ends or if that gap is less than 1cm. This avoids excessive tension over the suture line, which has been shown to negatively affect functional outcomes [3, 4]. Complex nerve injuries with gaps of greater than 1cm can be repaired using interposition autologous nerve grafts. Donor nerve, however, is a limited resource. Moreover, its harvest results in a functional deficit at the donor site and can be associated with donor-site morbidity, such as pain, infection, or neuroma formation [5]. The use of cadaveric nerve allograft has been shown to be effective in the repair of peripheral nerve defects up to 5cm in length [6]. One advantage to nerve allografts in longer gaps is their ability to provide an internal structure and extracellular matrix that serve as a scaffold to support directional migration of reparative Schwann cells. Cadaveric nerve, however, may be associated with immunologic responses, including graft vs. host disease, or transmission of human pathogens. Recently, improvements have been

made in the processing techniques used to prepare cadaveric nerve, resulting in improved removal of immunogenic elements while preserving fascicular architecture [7]. Currently available collagen and poly(lactic-co-glycolic acid) (PLGA) nerve conduits can be effective in the repair of short segment peripheral nerve injuries. Empty collagen conduits, for example, have reported effective repair lengths ranging from 1cm [8] to less than 3cm [9]. However, as the length of the defect increases, the efficacy of these empty nerve conduits declines, likely because they are unable to mimic the native internal architecture of the nerve and provide no internal scaffolding to support nerve regeneration.

Due to the shortcomings associated with these approaches to nerve repair, the development of bioengineered nerve conduits that can serve as nerve graft substitutes in the setting of complex nerve injury has been an active area of focus in tissue engineering research. Specifically, the ideal bioengineered nerve construct should not only mimic the aligned architecture of native nerve anatomy to support directional axonal regeneration, but should also provide the vital components of bioactivity found in the native extracellular matrix that facilitate Schwann cell attachment, proliferation, migration, and function.

In this study, we investigate the use of aligned nanofiber gels formed by self-assembling peptide amphiphiles (PA) in peripheral nerve regeneration [10, 11]. Because of their unique properties and molecular design, PA nanofibers can mimic the internal fascicular architecture of peripheral nerves, allow for the incorporation of Schwann cells vital for peripheral nerve regeneration, induce cellular and neurite alignment, and guide cell migration [12]. Moreover, the PAs can be engineered to possess bioactivity that is relevant to nerve regeneration. A PA presenting the amino acid sequence IKVAV (derived from laminin) has been shown to induce neural stem cell differentiation, stimulate neurite outgrowth, and lead to functional improvement in acute spinal-cord injury [13, 14]. The amino acid sequence RGDS is found naturally on molecules of fibronectin (and other proteins) and PAs bearing this sequence have been shown to promote cellular motility, proliferation, and differentiation *in vitro* [15-21]. Here we present our experience with the use of aligned PAs in both *in vitro* and *in vivo* models of peripheral nerve regeneration.

2. Materials and Methods

2.1. Rat Schwann cells cultures

Cells were purchased from ATCC (cell line RT4-D6P2T) and cultured in Dulbecco's Modified Eagle's Medium (DMEM) with 10% fetal bovine serum (FBS). Cells were cultured to confluence, treated with 0.25% trypsin, centrifuged, and resuspended in PBS for a final concentration of 3,500 cells/μL for WST-1 proliferation assays and 10,000 cells/μL for immunocytochemistry (ICC).

2.2 Backbone-PA and Bioactive PA gels

In order to synthesize the backbone-PA (consisting of only palmitoyl-VVAAEE-NH$_2$), the molecule was dissolved in aqueous 150 mM NaCl, 3 mM KCl, and NaOH solution to obtain a final 1 wt% solution at a pH between 7.2-7.4. In order to fabricate mixtures containing epitope-bearing PAs IKVAV and RGDS (consisting of palmitoyl-VVAAEE-NH$_2$ with

appended peptides, either RGDS (Arg-Gly-Asp-Ser) or IKVAV (Ile-Lys-Val-Ala-Val))**,** the backbone-PA was dissolved in aqueous 150mM NaCl, 3mM KCl, and NaOH solution to obtain a 1.33 wt% solution at a pH between 7.2-7.4. The epitope-containing PA was then dissolved with the same solution to obtain a 1 wt% solution at a pH between 7.2-7.4. The 1.33 wt% PA solution was then mixed in a 3:1 ratio with the 1% bioactive epitope solution creating a final bioactive-PA solution of 1 wt% PA and 0.25 wt% bioactive epitope. The three resulting solutions (backbone-PA, RGDS-PA, and IKVAV-PA) were then heated to 80 °C for 30 min in a water bath and left in the bath for slow cooling to 37 °C overnight [10, 11].

2.3 Combining Backbone-PA and Bioactive PA with Schwann cells

Following completion of the slow cooling, each of the PA solutions was mixed with Schwann cell suspension in a 4:1 ratio. A final cell density of 3,500 cells/μl was used for the WST-1 proliferation assays and 10,000 cells/μl for immunocytochemistry studies.

2.4. Backbone-PA and Bioactive PA-cell gel fabrication

A 200 μl volume of gelling solution consisting of 20 mM $CaCl_2$, 150 mM NaCl, and 3 mM KCl was pipetted onto a glass slide to form a thin film. The PA-Schwann cell suspensions were then pipetted in 4μl aliquots onto the thin film, instantly forming a string-like gel, with cells encapsulated within. These cell-embedded gels were maintained free floating in DMEM with 10% FBS in culture plates and incubated at 37 °C. Medium was changed every 72 hrs.

2.5. Collagen gels

Volumetric ratios of 1μl HEPES, 10 μl 10XPBS, 87 μl Collagen 10 mg/mL, and 2 μl Schwann cell PBS suspension were combined and mixed gently. Final cell density of 3,500 cells/μl was used for the WST-1 proliferation assays and 10,000 cells/μl, for immunocytochemistry studies. The mixture was then pipetted into a culture well (either a 96-well plate or 2-welled microscopy slides), and after 1 hour of curing and solidification at 37 °C, medium was added gently to the wells and changed every 3 days.

2.6. WST-1 proliferation assay

To evaluate the viability of cells within the gels, WST-1 reagent (Roche Applied Science, Indianapolis, IN, USA) was used for each PA-cell and collagen gel-cell complex. WST-1 assay has been widely used to measure cell proliferation. Aligned PA-cell gels along with collagen-cell gels were fabricated through the aforementioned methods at a final cell density of 3,500 cells/μl. Gels were then cultured in 96-well plates for various time periods (days 1, 7, 14, and 21). Following each time point, gels were incubated for 90 minutes in medium containing 10% WST-1 assay reagent. Following incubation, 100 μL of the conditioned medium were then transferred to a 96-well reading plate, and absorption values were read in a spectrophotometer at 450 nm. Measurements were repeated in sets of four.

2.7. Immunocytochemistry

PA-cell gels along with collagen-cell gels were fabricated through the aforementioned methods at a final cell density of 10,000 cells/μl. These gels were then cultured for 48 hours in 2-well microscopy slides, followed by fixation with 10% formalin and staining with mouse anti-vinculin monoclonal antibody (Abcam, Cambridge, MA), followed by FITC-conjugated anti-mouse secondary antibody (Abcam). Actin filaments were stained with rhodamine phalloidin (Life Technologies, Carlsbad, CA). Specimens were then viewed with confocal microscopy (Confocal SP1 MP-Inverted, Leica Microsystems Inc., Buffalo Grove, IL) using oil magnification, and images were recorded.

2.8. Preparation of PLGA Tube

Poly (lactide-co-glycolide acid) (PLGA) (75:25 mole ratio of D, L-lactide to glycolide, 0.76 dL/g, Lakeshore Biomaterials, Birmingham, AL) tubes were created using a modified gas foaming technique initially described by Mooney et al. [22]. PLGA microspheres were prepared with dichloromethane in water emulsion technique. A 1:7 weight ratio mixture of PLGA microspheres and NaCl particles (38-63 μm) were loaded into the annular gap of two glass tubes having an outside diameter of 3mm and inside diameter of 1.7mm. The powder mixture was manually packed using another glass tube having the same dimension as the annular gap. The materials were then equilibrated with high pressure CO_2 gas (800 psi) for 16 h in a custom-made pressure vessel. Afterwards, the pressure was released over a period of 45 min, which fused adjacent microspheres creating a continuous polymer structure. The NaCl porogen was leached for 6hrs hours in sterile milli-Q water. The tubes were then freeze dried overnight.

2.9. Incorporation of Aligned PA gel

The porous PLGA tubes were then loaded with an aligned PA gel (Fig. 1). This was achieved by placing the PLGA tube inside a 3mm ID glass tube. Then, using a smaller 1.7mm ID glass tube, a 40um pore size mesh-screen was fitted at the entrance of the PLGA tube. A syringe with a silicone tube fitting was used to force the PA nanofiber solution through the mesh screen, and inside the PLGA tube (Fig. 1)**.** Annealed PA nanofiber solutions behave as liquid crystals having many microdomains of fiber alignment, which can be oriented unidirectionally through shear and elongational flow **[10]**. The liquid crystal-like PA solution experiences significant shear forces as it passes through the mesh screen, and the nanofibers respond by aligning in the direction of fluid flow. After the aligned PA nanofiber solution filled the PLGA tube, the entire glass tube containing the materials was submerged in a 20mM $CaCl_2$ bath for 30 minutes allowing the PA solution to gel, thus trapping the nanofiber alignment in a gelatinous state. The PLGA/PA construct was then removed from the glass and cut to length, 12mm, and stored at 4°C for no longer than one week before implantation. Fabrication of backbone-PA and bioactive PA constructs followed the same protocol.

2.10. SEM and birefringence imaging

In preparation for SEM imaging, PLGA/backbone-PA constructs were first cut in half lengthwise using a thin razorblade in order to expose the aligned backbone-PA gel within

the PLGA shell. The sample was fixed in 3% glutaraldehyde for 20 min, and dehydrated in a series of EtOH washes. Samples were then critically point dried, mounted, and coated with 5 nm of osmium before imaging using a LEO Gemini 1525 sFEG SEM.

The fiber alignment was also visualized using birefringence. Constructs were first embedded in an agarose gel block and manually sectioned into ~0.5 mm slices cut parallel to the tube's long axis. These segments were laid flat in a glass dish filled with water and examined between two perpendicular light polarizers using an inverted Nikon Eclipse TPA00 Inverted Microscope.

2.11. Sciatic nerve defect

Animal procedures and protocols were reviewed and approved by the Animal Research Committee of the University of California Los Angeles. Sprague Dawley rats (average weight: 250 g) were purchased from Charles River Laboratories (Wilmington, MA, USA) and were housed and maintained at the UCLA vivarium under the care of the veterinary staff, according to the regulations set forth by the UCLA Office of Protection of Research Subjects. The rats were anesthetized using inhaled 2.5% isoflurane and the skin overlying the expected course of the sciatic nerve along the femur was trimmed of hair and prepped for surgery. An incision was made at the thigh and the sciatic nerve was carefully exposed and isolated within the inter-muscular space. Soft tissues surrounding the nerve were dissected to alleviate any proximal or distal tension on the nerve trunk. Using a surgical microscope and microsurgical instruments, a 12 mm segment of the nerve was carefully measured and then excised. (Fig. 2A) The resultant defects were reconstructed according to the following conditions: 1) no repair (negative control): the defects were left unrepaired and the proximal and distal cut ends were sutured to surrounding adventitia to prevent nerve migration (Fig 2B); 2) autograft (positive control): the resected nerve segment was immediately sutured back *in situ* (Fig. 2C); 3) empty conduit: a hollow 12mm sleeve of PLGA was sutured to the proximal and distal ends of the defect; 4) PLGA/backbone-PA construct: a 12mm segment of this construct was sutured to the proximal and distal ends of the defect; or 5) PLGA/RGDS-PA construct: a 12mm segment of this construct was sutured to the proximal and distal ends of the defect (Fig. 2D). The wound was then closed in layers, including muscle and skin. All the animals were kept under standardized laboratory conditions in an air- conditioned room with free access to food and water.

2.11. Sciatic Function Index

Motor functional recovery following the sciatic nerve injury was assessed using rat walking track analysis and footprint recording. The Sciatic Function Index (SFI) was calculated using the following formula:

$$SFI = 109.5\,(ETS - NTS)\,/NTS - 38.3\,(EPL - NPL)\,/NPL + 13.3\,(EIT - NIT)\,/NIT - 8.8 \quad [23],$$

where EPL indicates the operated experimental paw length; NPL, normal paw length; ETS, operated experimental toe spread, i.e., the distance between the first and fifth toes; NTS, the normal toe spread; EIT, the operated experimental inter-mediary toe spread, i.e., the distance between the second and fourth toes; and NIT, normal intermediary toe spread. Evaluations

of all animals were performed by a single investigator blinded to the experimental repair conditions.

2.12. Thermal sensitivity test

Sensory functional recovery following sciatic nerve injury was assessed using thermal sensitivity testing performed according to previously reported methods [24]. The Hargreaves paw withdrawal apparatus (Hargreaves Model 390, IITC Instruments) was used to measure the withdrawal latency from a radiant heat source directed at the proximal half of the plantar surface of each hind paw. Prior to testing, rats were allowed to acclimate for 10 minutes to the testing environment: a translucent plastic-walled individualized chamber ($10\times20\times20$ cm) with a 3mm thick glass bottom that was preheated to $30°C$. A radiant heat source consisting of an adjustable infrared lamp and a built-in stopwatch accurate to 0.1 s were used to measure paw withdrawal latency. Each paw was tested three times at 25% maximal heat intensity, with 5 minutes between each test. The test was performed only when a rat was stationary and standing on all four paws. Special care was taken to keep the glass bottom clean and dry during the testing. If the glass needed to be cleaned during the experiment, the rats were allowed 5–10 minutes to reacclimatize to the environment. The results of three tests were averaged for each paw.

2.13. Histological evaluations and quantitative analysis

The rats were euthanized using carbon dioxide followed by decapitation at week 12 following surgery. The sciatic nerve was re-exposed and harvested. The nerve specimens were fixed in 4% formaldehyde for 48 hours, embedded in paraffin, and cut into 4mm sections. These were then stained with conventional hematoxylin-eosin. Immunohistochemistry was also performed. Mouse monoclonal antibody to rat neurofilament (anti-NF, 1:1000 dilution; Abcam, Cambridge, MA) and S100 (1:2000 dilution; Sigma-Aldrich, St. Louis, MO) were applied overnight at $4°C$, respectively. The signal was detected using the mouse DAKO horseradish peroxidase (Dako Corporation, Carpinteria, CA) and visualized with the diaminobenzidine reaction. The sections were counterstained with hematoxylin. The numbers of NF or S-100 positive cells were counted per square area (100×100 μm) using ImageJ software (National Institute of Health, Bethesda, MD). Quantitative analyses of slides representing the various experimental conditions were compared.

2.14. Statistical Analysis

A one-way analysis of variance (ANOVA) was used to compare groups. The Tukey-Kramer multi-comparison adjustment was used as the post-hoc test to calculate the significance levels. $p < 0.05$ was considered statistically significant.

3. Results

3.1. Morphology of aligned PA gel

Direct observation of nanofiber alignment within the PLGA/backbone-PA construct is shown in the SEM micrograph in Fig. 3A. The vast majority of the nanofibers are oriented parallel with the tube axis, with only a few short fibers having another orientation. During

sample preparation a razor blade was used to expose the gel surface, so there is the possibility that the surface fiber orientation was perturbed by the sectioning process. Therefore, it was necessary to confirm this observed alignment using birefringence and small angle x-ray scattering (SAXS).

Fig. 3B shows the bright-field and birefringence microscopy of the backbone-PA gel within the construct. In this cross polarizer setup, all nanofiber domains oriented vertically and horizontally should appear dark, while diagonally oriented fiber domains should be bright. As expected, the backbone-PA area appears bright, indicating diagonal nanofiber orientation in the same direction of the tube's long axis.

Further proof of the aligned nanofiber morphology can be seen in the SAXS data shown in Fig. 3C. The same sectioned sample viewed in Fig. 3A was position in the path of the X-ray beam with the long axis of the construct oriented vertically. Figures 3Ca and b show the SAXS patterns obtained from the aligned construct and a non-aligned backbone-PA gel, respectively. The pinched profile in Fig. 3Ca reveals that the sample is very anisotropic and has a fiber alignment in the vertical direction. This alignment was obtained during fabrication when the backbone-PA fibers are sheared as they pass through the mesh screen. Without this shearing process the backbone-PA gel will have the isotropic SAXS profile shown in Fig. 3Cb**.**

3.2. Schwann cell proliferation in PA or collagen gels

Schwann cells demonstrated increasing proliferation with time when cultured in collagen and in backbone and bioactive PA gels (Fig. 4). Viability measurements at day 1 demonstrated that Schwann cells proliferated more rapidly in both IKVAV-PA and RGDS-PA gels compared to backbone-PA gel. By 7 days, proliferation in both IKVAV-PA and RGDS-PA were each significantly higher than that in backbone-PA gel. Proliferation in RGDS-PA gel was the highest among all groups, continuing to grow through 21 days of culture. Growth in IKVAV-PA was maximal at day 14, with neither significant expansion nor contraction of growth observed at day 21. Based upon these observations, RGDS-PA was chosen for use in all subsequent *in vivo* experimental groups treated with bioactive PA.

3.3. Cytoskeletal assessment and focal adhesion protein stain

The effect of the aligned PA gels on the spatial arrangement of cytoskeletal actin was examined using actin stain (Fig. 5). Schwann cells were well-spread and randomly oriented with respect to their cytoskeletal elements in 2D culture or in a collagen gel. On the other hand, significant cytoskeletal alignment and cellular elongation were observed in aligned PA gels. There was no significant difference in actin appearance when comparing RGDS-PA and IKVAV-PA gels. Vinculin immunostaining was performed for Schwann cells to visualize the exact location of focal adhesion sites. Vinculin-positive sites were observed on all aligned PA gels.

3.4. Latency to hind paw withdrawal from a thermal stimulus after sciatic nerve defect reconstruction

Fig. 6 shows typical gross observations of sciatic nerve in the various experimental groups 12 weeks after surgery. In the negative control group, no nerve regeneration was observed (Fig. 6A). On the other hand, nerve growth was observed in the autograft group (Fig. 6B) and PLGA/RGDS-PA construct group (Fig. 6C). PLGA conduit was degraded completely during the postoperative period as anticipated (Fig. 6C).

Fig. 7 shows the time profile of latency to hind paw withdrawal from a thermal stimulus after various treatments of sciatic nerve defects. The unoperated limb of each experimental animal was used as a control. The average time for the control hind paw to withdraw from a thermal stimulus measured consistently between 4-6 seconds throughout the testing period. Significant increases in reaction time were seen in all hind paws that received sciatic nerve transection on day 0. Improvement in this time was observed beginning on postoperative day 7 for the PLGA/backbone-PA and PLGA/RGDS-PA construct groups and on day 14 for the autograft group. The empty conduit group did not show significant improvement until day 28. Ultimately, all treatment groups recovered to a baseline level of function relative to controls, except for the defect group, in which stimulus response times remained elevated.

3.5. Motor function recovery after sciatic nerve defect reconstruction

We assessed the motor function recovery using the walking track analysis and SFI. Results are shown for autologous repair, empty conduit, PLGA/backbone-PA, and PLGA/RGDS-PA in Figure **8**. An SFI value of −100 represents complete impairment, whereas a value near 0 indicates normal motor function [25]. Our negative control animals that received a critical sized sciatic nerve defect without any repair constantly showed SFI values of −100 throughout the entire 12 week period of testing, indicating no sciatic nerve motor recovery. Notably, PLGA/backbone-PA and PLGA/RGDS-PA construct groups showed early improvement within 4 weeks, comparable to the autologous group. Furthermore, the SFI values in the PLGA/RGDS-PA group showed statistically significant improvement 4 weeks after the surgery compared to that of the empty conduit group, and levels that were comparable to the autograft group.

3.6. Histological findings and quantitative analysis

At 12 weeks, rats were euthanized and the sciatic nerve specimens were harvested. Transverse sections of the regenerated nerve in each group were stained with Hematoxylin-Eosin (Fig. 9A), anti-NF antibody to evaluate axonal regeneration (Fig. 9B), and anti-S-100 antibody for Schwann cells (Fig. 9C). The density of regenerated axons in the center of the regenerate nerve was higher in both PLGA/backbone-PA and PLGA/RGDS-PA construct groups relative to the empty PLGA conduit group. Furthermore, the axonal arrangement in these two groups was similar to that of the Autograft group. Only a few nerve fibers grew along the empty conduit, and the arrangement of the regenerated nerve fiber was attenuated in the empty tube. As shown in Fig. 9C, PLGA/backbone-PA and PLGA/RGDS-PA construct groups exhibited S-100-positive staining cells 12 weeks after the surgery, demonstrating the regeneration and re-population of Schwann cells within the bioengineered nerve constructs. Quantitative analysis also shows that the number of NF positive cells and

S-100 positive cells in the regenerate nerve was higher in both PLGA/backbone-PA and PLGA/RGDS-PA construct groups relative to the empty PLGA conduit group (Fig. 9D). These data suggested that the regeneration and migration of Schwann cells played a key role in the successful axonal regeneration of the critical size peripheral nerve gap.

4. Discussion

The natural anatomy of a peripheral nerve fiber provides the basis for its regeneration in the setting of injury. The outer epineurial layer maintains nerve fiber integrity and assists with its incorporation into the surrounding soft tissues, while the internal fascicular structure supports axonal guidance, function and proliferation. On the molecular level, bioactive extracellular matrix (ECM) molecules, in particular laminin and fibronectin, play a crucial role in stimulating various cellular activities that are integral to regeneration and facilitating Schwann cell migration, and proliferation, which is critical for neurite outgrowth [26]. These molecules also provide binding sites and directional guidance for growing axons.

Much research on peripheral nerve regeneration has focused on the development of nerve conduits for guided nerve regeneration. Axons sprout from the proximal end of the transected nerve end and grow into the conduit, which bridges the nerve gap. The conduit serves to guide and protect the nerve regenerate as it approaches the distal end of the cut nerve. Currently, PLGA-based and collagen-based conduits are commercially available for use in peripheral nerve repair in humans. However, the efficacy of these empty conduits is limited to short distance nerve gaps, on the order of 1cm to less than 3cm [8]. Beyond that length, the efficacy of nerve repair using a conduit declines with increasing nerve gap size. Acellular cadaveric nerve allografts have been reported to be effective in defects up to at least 5cm in length [9]. We hypothesize that the difference in effectiveness between empty conduits and nerve allograft lies in the internal architecture provided by the latter: an aligned three-dimensional scaffold can facilitate neurite migration better than a hollow tube.

Based upon this notion, and with our knowledge that nerve regeneration is also dependent upon a nurturing wound milieu, we propose that the ideal nerve graft substitute should include a linearly oriented matrix that mimics the internal fascicular structure of native peripheral nerve and presents bioactive factors that support the attachment, proliferation, and migration Schwann cells and neurons [27, 28].

Previous attempts to design a bioengineered nerve construct that mimics the three-dimensional architecture of a natural nerve fiber have included the use of aligned phosphate glass fibers [29], as well as other aligned biomaterials [30-32]. High surface area to volume ratios have been shown to facilitate the cell migration required to bridge peripheral nerve gaps [30]. Electrospinning has recently been used to create three-dimensional conduits for peripheral nerve regeneration through the fabrication of supporting nanofiber mesh [33]. Bi-layered electrospun conduits, designed with a luminal longitudinally aligned layer and an outer randomly oriented layer, have been shown to effect better long term *in-vivo* results compared to randomly oriented electrospun conduits [11], emphasizing the potential clinical benefit of an aligned inner layer. Electrospinning, however, relies on a high-energy process and requires the use of organic solvent, the cytotoxic effects of which make it exceedingly

difficult to include viable cells in the construct during the fabrication process. The combination of stem cell therapy with this approach to biomaterial fabrication is therefore limited. Additionally, the mesh nanofibers, while providing gross physical cellular support, may not actively induce aligned and directed cell growth, nor do they have the capacity to present any bioactive molecules that are native to the ECM and that may stimulate stimulating the cellular functions needed for peripheral nerve regeneration.

PA nanofibers by comparison represent a biomaterials platform with great promise in addressing the requirements that need to be met in the design of a nerve graft substitute. Every PA molecule consists of 4 functional segments: 1) A hydrophobic alkyl tail (e.g. palmitoyl) that drives aggregation through hydrophobic collapse; 2) a beta-sheet-forming peptide sequence (e.g. VVAA) that promotes nanofiber formation and influences the fiber mechanical properties; 3) ionizable side-chain residues that render PAs soluble in aqueous solutions (e.g. E); and 4) a bioactive epitope sequence that can interact with cellular receptors and stimulate cellular activities. Upon thermal treatment, certain PA sequences (e.g. VVAAEE) form liquid crystal-like fiber bundles that can be aligned upon application of a gentle shear (similar to that of pipetting). Aligned PAs are able to gel in the presence of salts with divalent cations (such as Ca^{2+}), and the forces required for alignment are much lower than with the high strain or flow rates required in electrospun internal scaffolds [10]. This physiologic fabrication process allows living cells to be cultured directly into the biomaterial as it undergoes gelation.

The benefits of the IKVAV (Ile-Lys-Val-Ala-Val) epitope have already been shown in spinal cord injury models [13, 14]. As an integrin binding sequence found on fibronectin, RGDS (Arg-Gly-Asp-Ser) exerts key biochemical influences on a variety of cells types including fibroblasts [15], osteoblasts [34, 35], and neurons [36]. Schwann cells are also influenced by interactions with fibronectin, and these cells are vital to axonal growth and elongation by creating the specific biochemical microenvironment needed for peripheral nerve regeneration. In particular, Schwann cells phagocytose axonal and myelin debris and elaborate chemoattractant molecules for macrophages that help in the same manner. It is likely that the naturally occurring RGDS sequences found in fibronectin plays a vital role in the stimulation and regulation of Schwann cell activity in the regeneration of peripheral nerve.

In our study, we have demonstrated that Schwann cells remain viable in aligned PA gels, and furthermore that Schwann cell proliferation in these gels is comparable to that seen in collagen conduit, including after 21 days of culture (Fig. 4). This result indicates that PAs may be used clinically in a bioengineered nerve graft construct without negative effects on the growth kinetics of the vital cellular components needed for peripheral nerve regeneration.

We have also shown that the addition of the use of bioactive PAs significantly increases the proliferation of Schwann cells (Fig. 4). Both IKVAV-PA and RGDS-PA increased proliferation of Schwann cells compared to backbone-PA for at least 14 days. This observation was persistent through 21 days in the RGDS-PA model, and is consistent with the fibronectin-like conformation of the RGDS epitope and its role as discussed above.

Based on this finding, RGDS-PA was used in our subsequent *in-vivo* nerve regeneration experimental groups.

While proliferation assays give us an idea of the health of the Schwann cells in three-dimensional *in vitro* culture, it is crucial to document that these cells are behaving in a manner that is consistent with their behavior in native nerve tissue. Although our proliferation assays demonstrate increasing proliferation, we cannot know if the resulting growth is organized in an aligned and guided fashion that is conducive to effective peripheral nerve regeneration. Through the use of immunocytochemistry (ICC), however, we demonstrated that Schwann cells orient along the aligned axis of PA gels (Fig. 5). While Schwann cells were able to grow and attach to collagen matrices in our control cultures, they did so in an unaligned fashion: cytoskeletal elements and process extensions were randomly oriented. In contrast, cells grown in aligned PA gels--both backbone-PA and bioactive PAs--demonstrated marked linear arrangement of their cytoskeletal elements, their pattern of growth, and their cellular extensions.

Our *in vivo* results further support the value of providing an internal scaffolding to the nerve regeneration construct. The rat sciatic nerve model is a widely recognized and implemented in the study of peripheral nerve injury [37]. While 10mm defects have been used previously by other groups [38], we elected to use a larger defect to mitigate any chance of spontaneous autologous repair. As our negative controls demonstrate, there was no return of sensory or motor function in animals with defects that were left unrepaired. Furthermore, histological examination of the surgical sites in negative control animals revealed no regeneration of nerve tissue within the critical defects 12 weeks after surgery.

While gastrocnemius weights are often used to determine the efficacy of sciatic nerve regeneration in experimental animal models, we elected not to study this variable, having confidence in our functional results, particularly as our *in vitro* and *in vivo* results were correlative. The SFI is frequently used in the assessment of peripheral nerve motor function as modeled using the rat sciatic nerve [39, 40] and the use of thermal sensitivity/ nocioception is also a commonly used assessment tool [41, 42]. Our bioengineered PLGA/ RGDS-PA constructs yielded return of motor function that was not only statistically improved from empty conduit, but that was also statistically comparable to results observed in animals treated with autologous nerve graft, the current gold standard in nerve repair therapy. There was a trend of improvement when comparing empty conduit to PLGA/ backbone-PA construct, but these differences were not statistically significant. Overall, our PLGA/RGDS-PA construct demonstrated a quicker return of motor function in experimental animals. Based on our *in vitro* data, we attribute this in part due to its potential ability to augment Schwann cell alignment, proliferation, and migration through its fibronectin-mimicking characteristics. If these vital regenerative cells are able to grow more quickly within the defect site, the optimal biochemical environment needed for nerve regeneration may develop more efficiently.

We noted similar results in our sensory function assessments. Thermal nocioceptive signals are conveyed via unmyelinated C fibers, which are responsible for the delayed sensation associated with heat-associated pain [43, 44]. In our model, we used latency time from

introduction of a thermal noxious stimulus (i.e., a burning sensation) to actual withdrawal of the hind paw from the heat source as a measure of intact sensory function. In unoperated control limbs, this time averaged 5 seconds (range 4-6 seconds). Interestingly, both the PLGA/backbone-PA and PLGA/RGDS-PA constructs demonstrated significantly faster return of sensory function compared to empty conduit, approaching test results seen in normal limbs after 30 days. Rate of recovery was also comparable to that seen in autologous reconstruction groups, and in fact was improved during the first week following surgery. Unreconstructed groups never saw return to normal latency times. These results further underscore the positive impact of an internally aligned architecture in the design of the nerve regeneration construct, again emphasizing the potential role of the bioactive PA epitope in supporting Schwann cell activity and subsequent functional outcomes.

Histological analysis of the reconstructed defect sites is consistent with our *in vivo* functional test findings. Both axons and Schwann cells were able migrate into and proliferate within the PLGA/backbone-PA and PLGA/RGDS-PA constructs, Notably, empty conduits demonstrated negligible axonal and Schwann cell migration. The architecture of the regenerate nerves in autologous and PA-based reconstructions was reminiscent of the native nerve architecture seen in histological specimens of unoperated nerve controls.

5. Conclusion

The creation of an ideal bioengineered nerve regeneration construct requires mimicry of the native nerve ultrastructure and bioactivity. These two components are vital for the optimal function of Schwann cells that participate in peripheral nerve regeneration and for the guided and directional growth of new nerve fibers. Aligned RGDS-PA gels are able to provide both the physical architecture and bioactivity necessary to promote Schwann cell proliferation, attachment, and alignment. We believe that this biomaterial represents a viable solution to the challenges we currently face in clinical peripheral nerve injury and repair. Future lines of study will involve the pre-population of this bioengineered nerve construct with cellular components, including pluripotent stem cells, as well as neurogenic growth factors, as we work towards development of a translational model based on the clinical potential of bioactive PAs.

Supplementary Material

Refer to Web version on PubMed Central for supplementary material.

Acknowledgments

References

[1]. Kehoe S, Zhang XF, Boyd D. FDA approved guidance conduits and wraps for peripheral nerve injury: a review of materials and efficacy. Injury. 2012; 43:553–72. [PubMed: 21269624]

[2]. Visser PA, Hermreck AS, Pierce GE, Thomas JH, Hardin CA. Prognosis of nerve injuries incurred during acute trauma to peripheral arteries. Am J Surg. 1980; 140:596–9. [PubMed: 7435813]

[3]. Millesi H. Microsurgery of peripheral nerves. Hand. 1973; 5:157–60. [PubMed: 4715701]

[4]. Naff NJ, Ecklund JM. History of peripheral nerve surgery techniques. Neurosurg Clin N Am. 2001; 12:197–209. x. [PubMed: 11175999]

[5]. Daly W, Yao L, Zeugolis D, Windebank A, Pandit A. A biomaterials approach to peripheral nerve regeneration: bridging the peripheral nerve gap and enhancing functional recovery. J R Soc Interface. 2012; 9:202–21. [PubMed: 22090283]

[6]. Ducic I, Fu R, Iorio ML. Innovative treatment of peripheral nerve injuries: combined reconstructive concepts. Ann Plast Surg. 2012; 68:180–7. [PubMed: 22270569]

[7]. Carriel V, Alaminos M, Garzon I, Campos A, Cornelissen M. Tissue engineering of the peripheral nervous system. Expert Rev Neurother. 2014; 14:301–18. [PubMed: 24506662]

[8]. Bushnell BD, McWilliams AD, Whitener GB, Messer TM. Early clinical experience with collagen nerve tubes in digital nerve repair. J Hand Surg Am. 2008; 33:1081–7. [PubMed: 18762101]

[9]. Evriviades D, Jeffery S, Cubison T, Lawton G, Gill M, Mortiboy D. Shaping the military wound: issues surrounding the reconstruction of injured servicemen at the Royal Centre for Defence Medicine. Philos Trans R Soc Lond B Biol Sci. 2011; 366:219–30. [PubMed: 21149357]

[10]. Zhang S, Greenfield MA, Mata A, Palmer LC, Bitton R, Mantei JR, et al. A self-assembly pathway to aligned monodomain gels. Nat Mater. 2010; 9:594–601. [PubMed: 20543836]

[11]. Berns EJ, Sur S, Pan L, Goldberger JE, Suresh S, Zhang S, et al. Aligned neurite outgrowth and directed cell migration in self-assembled monodomain gels. Biomaterials. 2014; 35:185–95. [PubMed: 24120048]

[12]. McClendon MT, Stupp SI. Tubular hydrogels of circumferentially aligned nanofibers to encapsulate and orient vascular cells. Biomaterials. 2012; 33:5713–22. [PubMed: 22591610]

[13]. Tysseling VM, Sahni V, Pashuck ET, Birch D, Hebert A, Czeisler C, et al. Self-assembling peptide amphiphile promotes plasticity of serotonergic fibers following spinal cord injury. J Neurosci Res. 2010; 88:3161–70. [PubMed: 20818775]

[14]. Silva GA, Czeisler C, Niece KL, Beniash E, Harrington DA, Kessler JA, et al. Selective differentiation of neural progenitor cells by high-epitope density nanofibers. Science. 2004; 303:1352–5. [PubMed: 14739465]

[15]. Houseman BT, Mrksich M. The microenvironment of immobilized Arg-Gly-Asp peptides is an important determinant of cell adhesion. Biomaterials. 2001; 22:943–55. [PubMed: 11311013]

[16]. Irvine DJ, Ruzette AV, Mayes AM, Griffith LG. Nanoscale clustering of RGD peptides at surfaces using comb polymers. 2. Surface segregation of comb polymers in polylactide. Biomacromolecules. 2001; 2:545–56. [PubMed: 11749219]

[17]. Irvine DJ, Mayes AM, Griffith LG. Nanoscale clustering of RGD peptides at surfaces using Comb polymers. 1. Synthesis and characterization of Comb thin films. Biomacromolecules. 2001; 2:85–94. [PubMed: 11749159]

[18]. Jensen TW, Hu BH, Delatore SM, Garcia AS, Messersmith PB, Miller WM. Lipopeptides incorporated into supported phospholipid monolayers have high specific activity at low incorporation levels. J Am Chem Soc. 2004; 126:15223–30. [PubMed: 15548019]

[19]. Massia SP, Hubbell JA. An RGD spacing of 440 nm is sufficient for integrin alpha V beta 3-mediated fibroblast spreading and 140 nm for focal contact and stress fiber formation. J Cell Biol. 1991; 114:1089–100. [PubMed: 1714913]

[20]. Maheshwari G, Brown G, Lauffenburger DA, Wells A, Griffith LG. Cell adhesion and motility depend on nanoscale RGD clustering. J Cell Sci. 2000; 113(Pt 10):1677–86. [PubMed: 10769199]

[21]. Rowley JA, Mooney DJ. Alginate type and RGD density control myoblast phenotype. J Biomed Mater Res. 2002; 60:217–23. [PubMed: 11857427]

[22]. Mooney DJ, Baldwin DF, Suh NP, Vacanti JP, Langer R. Novel approach to fabricate porous sponges of poly(D,L-lactic-co-glycolic acid) without the use of organic solvents. Biomaterials. 1996; 17:1417–22. [PubMed: 8830969]

[23]. Bain JR, Mackinnon SE, Hunter DA. Functional evaluation of complete sciatic, peroneal, and posterior tibial nerve lesions in the rat. Plast Reconstr Surg. 1989; 83:129–38. [PubMed: 2909054]

[24]. Matsuka Y, Ono T, Iwase H, Mitrirattanakul S, Omoto KS, Cho T, et al. Altered ATP release and metabolism in dorsal root ganglia of neuropathic rats. Mol Pain. 2008; 4:66. [PubMed: 19108746]

[25]. Kanaya F, Firrell J, Tsai TM, Breidenbach WC. Functional results of vascularized versus nonvascularized nerve grafting. Plast Reconstr Surg. 1992; 89:924–30. [PubMed: 1561263]

[26]. Armstrong SJ, Wiberg M, Terenghi G, Kingham PJ. ECM molecules mediate both Schwann cell proliferation and activation to enhance neurite outgrowth. Tissue Eng. 2007; 13:2863–70. [PubMed: 17727337]

[27]. Schmidt CE, Leach JB. Neural tissue engineering: strategies for repair and regeneration. Annu Rev Biomed Eng. 2003; 5:293–347. [PubMed: 14527315]

[28]. de Ruiter GC, Malessy MJ, Yaszemski MJ, Windebank AJ, Spinner RJ. Designing ideal conduits for peripheral nerve repair. Neurosurg Focus. 2009; 26:E5. [PubMed: 19435445]

[29]. Kim YP, Lee GS, Kim JW, Kim MS, Ahn HS, Lim JY, et al. Phosphate glass fibres promote neurite outgrowth and early regeneration in a peripheral nerve injury model. J Tissue Eng Regen Med. 2012 Epub ahead of print.

[30]. Neal RA, Tholpady SS, Foley PL, Swami N, Ogle RC, Botchwey EA. Alignment and composition of laminin-polycaprolactone nanofiber blends enhance peripheral nerve regeneration. J Biomed Mater Res A. 2011 Epub ahead of print.

[31]. Jiang X, Mi R, Hoke A, Chew SY. Nanofibrous nerve conduit-enhanced peripheral nerve regeneration. J Tissue Eng Regen Med. 2012 Epub ahead of print.

[32]. Jin J, Park M, Rengarajan A, Zhang Q, Limburg S, Joshi SK, et al. Functional motor recovery after peripheral nerve repair with an aligned nanofiber tubular conduit in a rat model. Regen Med. 2012; 7:799–806. [PubMed: 23164080]

[33]. Zhu Y, Wang A, Patel S, Kurpinski K, Diao E, Bao X, et al. Engineering bi-layer nanofibrous conduits for peripheral nerve regeneration. Tissue Eng Part C Methods. 2011; 17:705–15. [PubMed: 21501089]

[34]. Secchi AG, Grigoriou V, Shapiro IM, Cavalcanti-Adam EA, Composto RJ, Ducheyne P, et al. RGDS peptides immobilized on titanium alloy stimulate bone cell attachment, differentiation and confer resistance to apoptosis. J Biomed Mater Res A. 2007; 83:577–84. [PubMed: 17503524]

[35]. Oh JH, Kim HJ, Kim TI, Baek JH, Ryoo HM, Woo KM. The effects of the modulation of the fibronectin-binding capacity of fibrin by thrombin on osteoblast differentiation. Biomaterials. 2012; 33:4089–99. [PubMed: 22386921]

[36]. Gunn JW, Turner SD, Mann BK. Adhesive and mechanical properties of hydrogels influence neurite extension. J Biomed Mater Res A. 2005; 72:91–7. [PubMed: 15536643]

[37]. Varejao AS, Melo-Pinto P, Meek MF, Filipe VM, Bulas-Cruz J. Methods for the experimental functional assessment of rat sciatic nerve regeneration. Neurol Res. 2004; 26:186–94. [PubMed: 15072638]

[38]. Niu Y, Chen KC, He T, Yu W, Huang S, Xu K. Scaffolds from block polyurethanes based on poly(varepsilon-caprolactone) (PCL) and poly(ethylene glycol) (PEG) for peripheral nerve regeneration. Biomaterials. 2014; 35:4266–77. [PubMed: 24582378]

[39]. Castaneda F, Kinne RK. Omental graft improves functional recovery of transected peripheral nerve. Muscle Nerve. 2002; 26:527–32. [PubMed: 12362419]

[40]. Wong BJ, Mattox DE. Experimental nerve regeneration. A review. Otolaryngol Clin North Am. 1991; 24:739–52. [PubMed: 1762787]

[41]. Varejao AS, Cabrita AM, Geuna S, Patricio JA, Azevedo HR, Ferreira AJ, et al. Functional assessment of sciatic nerve recovery: biodegradable poly (DLLA-epsilon-CL) nerve guide filled with fresh skeletal muscle. Microsurgery. 2003; 23:346–53. [PubMed: 12942525]

[42]. Masters DB, Berde CB, Dutta SK, Griggs CT, Hu D, Kupsky W, et al. Prolonged regional nerve blockade by controlled release of local anesthetic from a biodegradable polymer matrix. Anesthesiology. 1993; 79:340–6. [PubMed: 8342843]

[43]. Millan MJ. The induction of pain: an integrative review. Prog Neurobiol. 1999; 57:1–164. [PubMed: 9987804]

[44]. Craig AD, Andrew D. Responses of spinothalamic lamina I neurons to repeated brief contact heat stimulation in the cat. J Neurophysiol. 2002; 87:1902–14. [PubMed: 11929910]
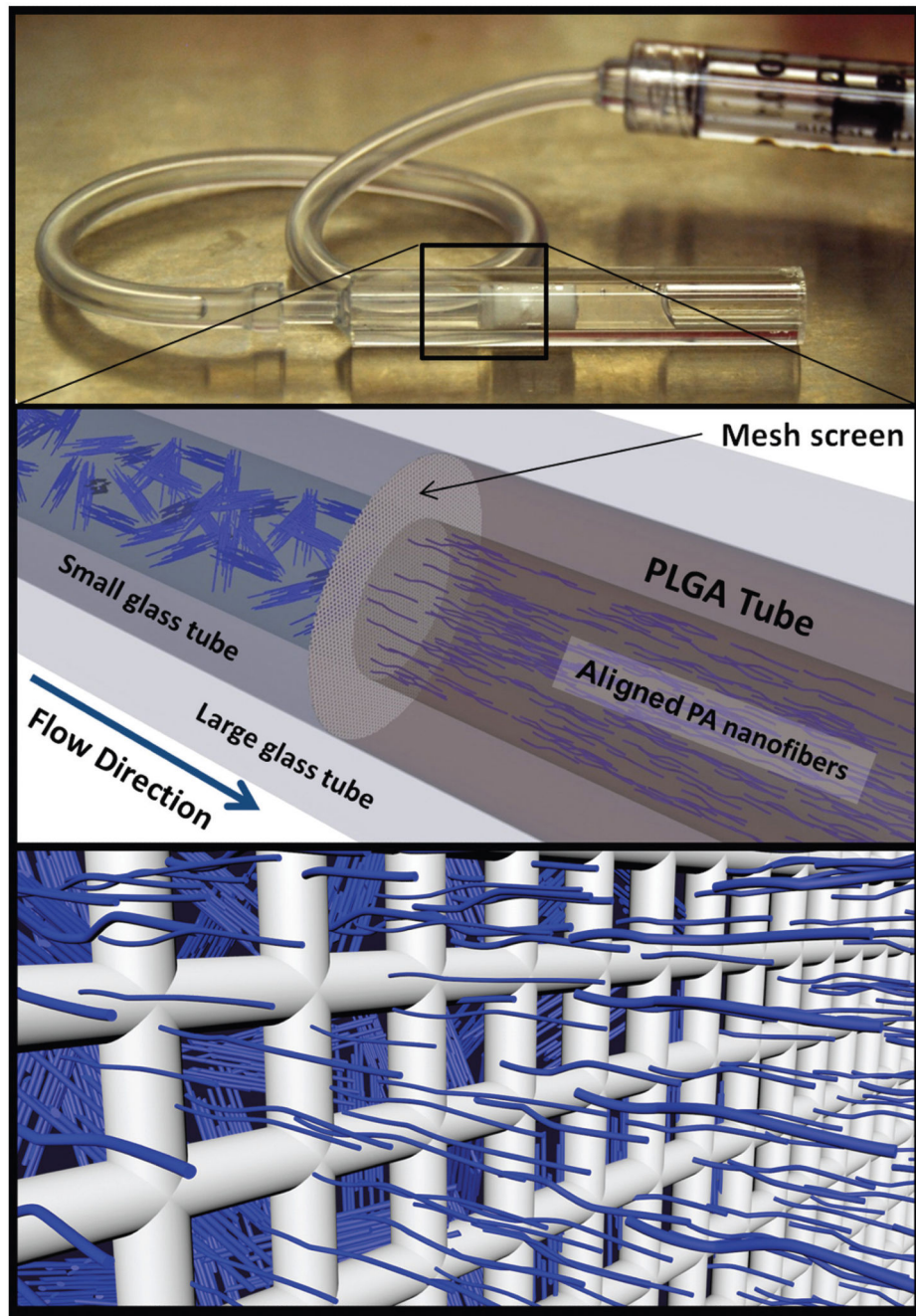
Fig. 1.
The PA solution is loaded into the PLGA tubes by first passing through a 40-μm mesh screen. The liquid crystalline behavior of nanofibers allows them to align in response to the shear flow experienced as they pass through the mesh. After the PA solution fills the PLGA tube the entire implant is submerged in a 20mM $CaCl_2$ bath, thus trapping the nanofiber alignment in a gel-state. Nanofiber size is exaggerated for graphical appeal.
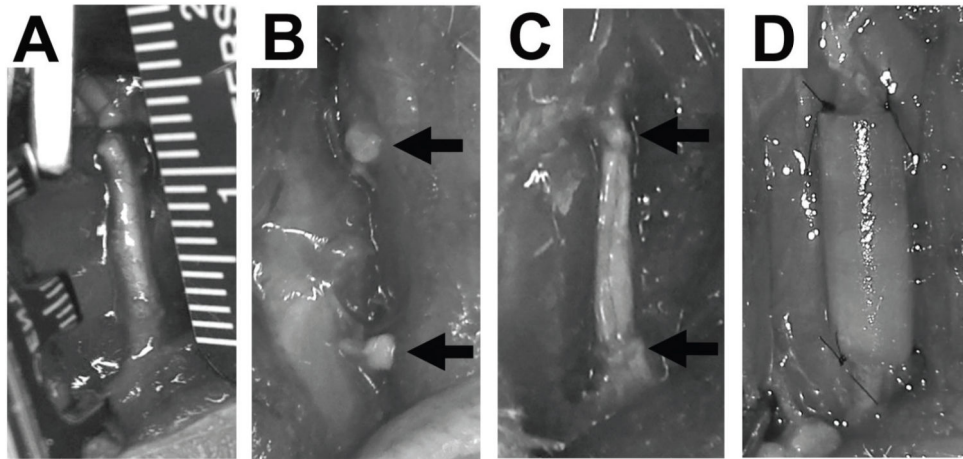
Fig. 2.
Gross images of sciatic nerve during the surgery. (**A**) Measurement of the 12 mm segment of nerve to be excised. (**B**) Transection of the sciatic nerve. Arrows indicate the proximal and distal nerve stumps, which are sutured to surrounding adventitia to prevent migration. (**C**) Resected nerve segment is sutured back in place as an autograft. Arrows indicate the proximal and distal nerve stumps. (**D**) The proximal and distal nerve segments are bridged using PLGA/backbone-PA or PLGA/RGDS-PA conduit between the two ends. Arrows indicate the proximal and distal nerve stumps.
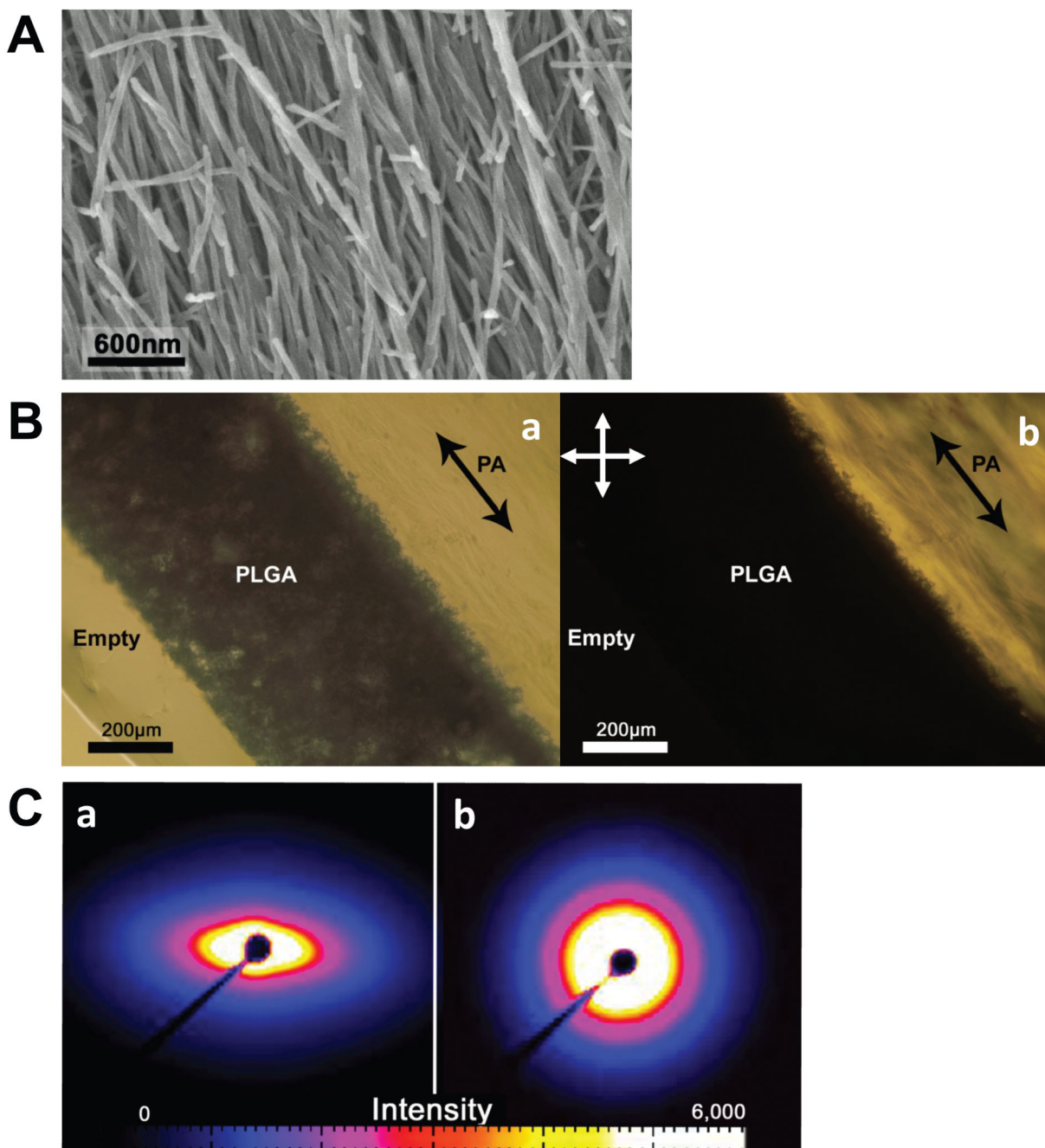
Fig. 3.
(**A**) SEM showing the aligned PA nanofibers inside the PLGA tube constructs. The tubes were cut in half along their long axis to expose the nanofibers. (**B**) ~0.5mm longitudinal section of the tube constructs is imaged using optical microscopy. **a**: Imaged under brightfield mode, the porous scaffold is shown with the inner PA gel on the right. **b:** Imaged between cross polars with orientation shown in the upper left, domains of nanofibers aligned diagonally appear bright while horizontal and vertical domains appear dark. The dark arrows indicate long axis of tubes. (**C**) **a:** The ~0.5mm tube section was probed using small angle

X-ray scattering (SAXS). The sample was oriented with the long axis vertical (see supplemental information). The SAXS pattern shows an obvious pinched profile indicating nanofiber alignment along the long axis of the tube. **b:** An unaligned gel was also probed to show contrast between aligned and non-aligned SAXS data.
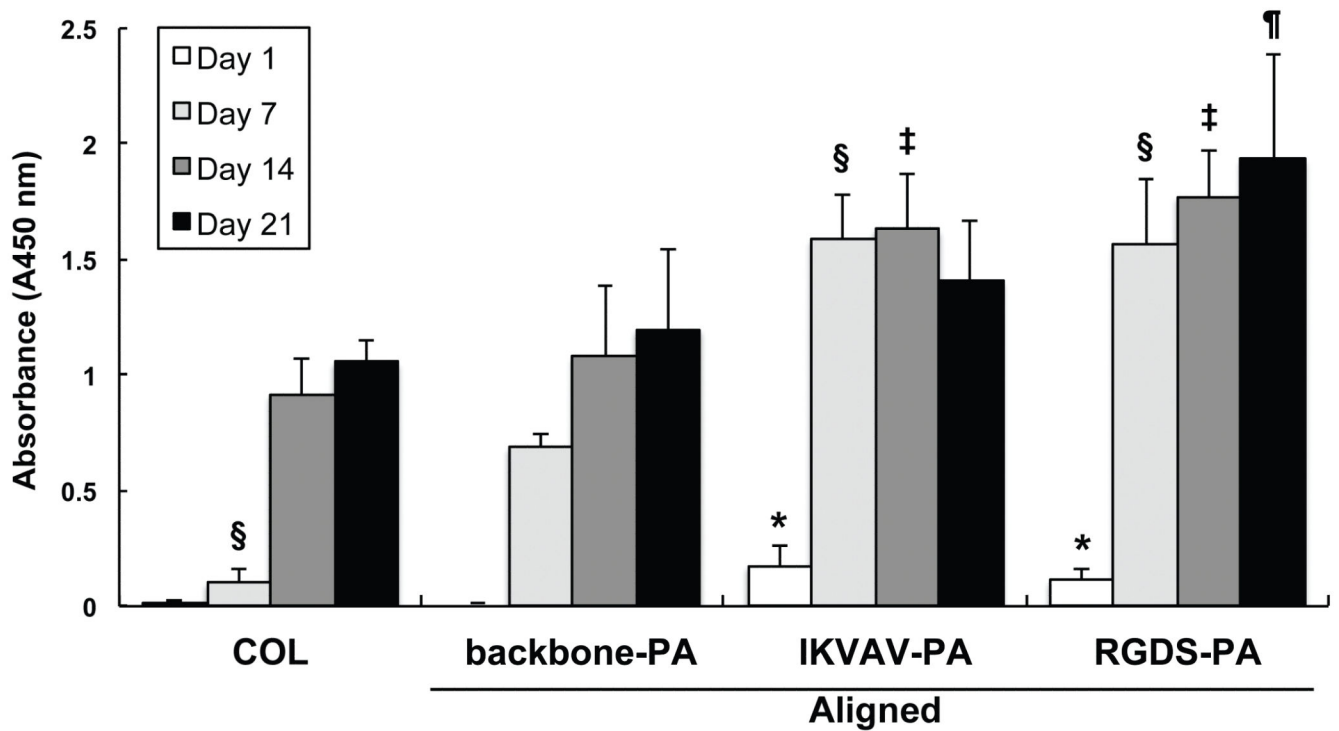
Fig. 4.
Schwann cell proliferation in various gels. IKVAV-PA statistically increased Schwann cell proliferation vs. backbone-PA up to Day 14; RGDS did so up to day 21. All p values were calculated using ANOVA and Tukey-Kramer test. * $p<0.05$ vs. backbone-PA at day 1. § $p<0.05$ vs. backbone-PA at day 7. ‡ $p<0.05$ vs. backbone-PA at day 14. ¶ $p<0.05$ vs. backbone-PA at day 21.
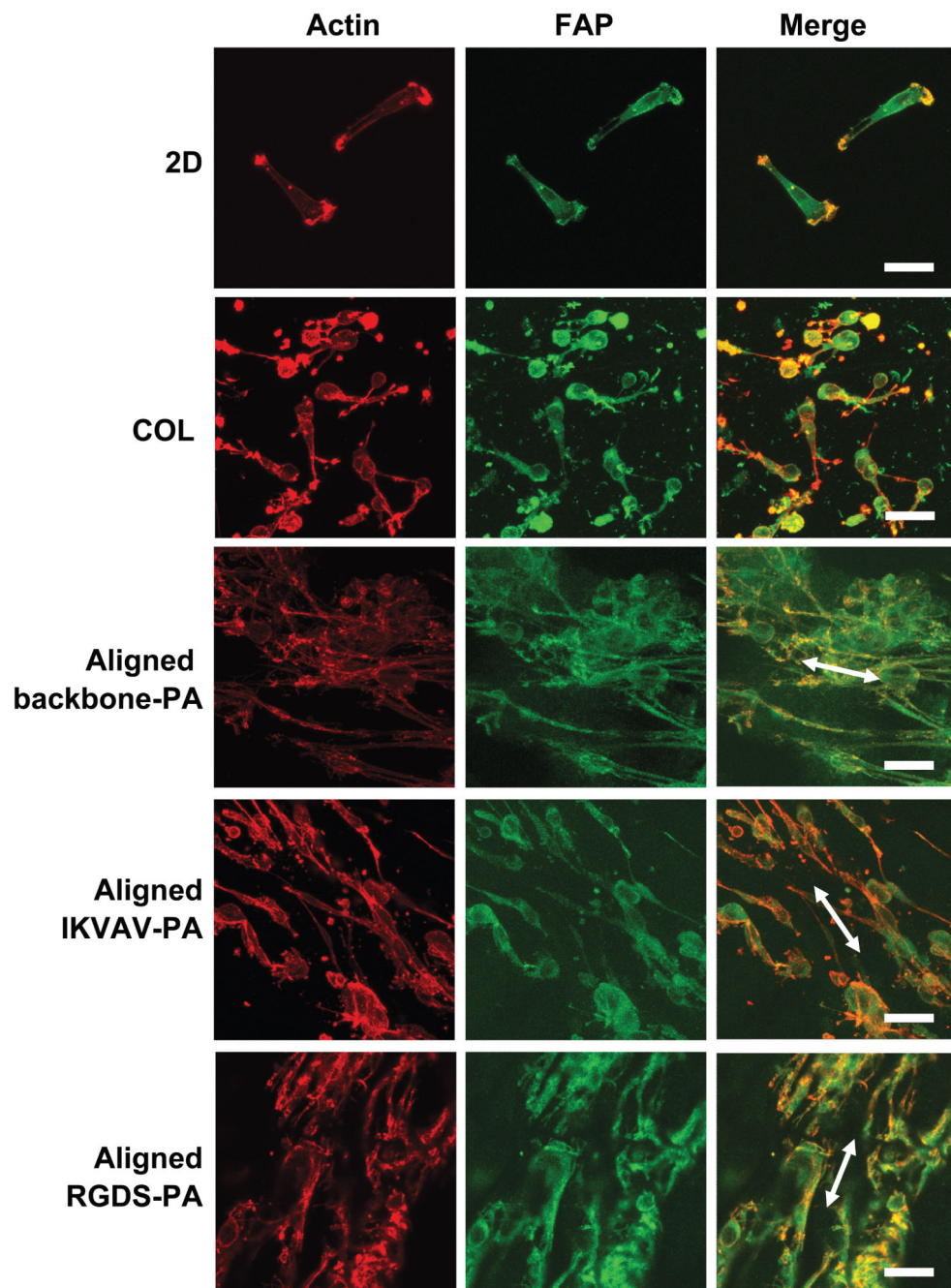
Fig. 5.
Immunocytochemistry of actin and focal adhesion protein (FAP) of Schwann cells on conventional 2D culture dish (2D), in collagen gel, aligned backbone-PA gel, aligned IKVAV-PA gel, or aligned RGDS-PA gel. The white arrows indicate the direction of the gel. Scale bar, 50 μm.
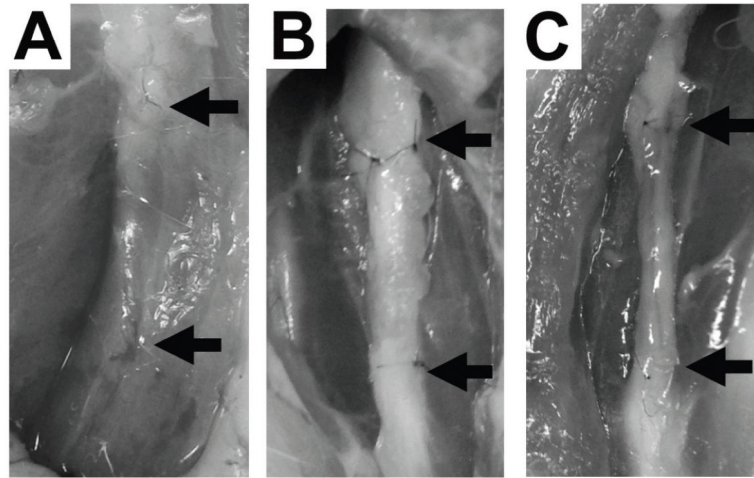
Fig. 6.
Gross observation of sciatic nerve 12 weeks after the surgery. (**A**) No nerve regeneration was observed in the negative control; scar tissue filled the original defect site. Arrow indicates the nerve stump. (**B**) Nerve bridging was observed in the Autograft group. Arrows indicate the original proximal and distal nerve stumps. (**C**) Nerve regeneration was observed in the PLGA/RGDS-PA group. PLGA conduit was degraded completely, leaving behind regenerate nerve structure. Arrows indicate the original proximal and distal nerve stumps.
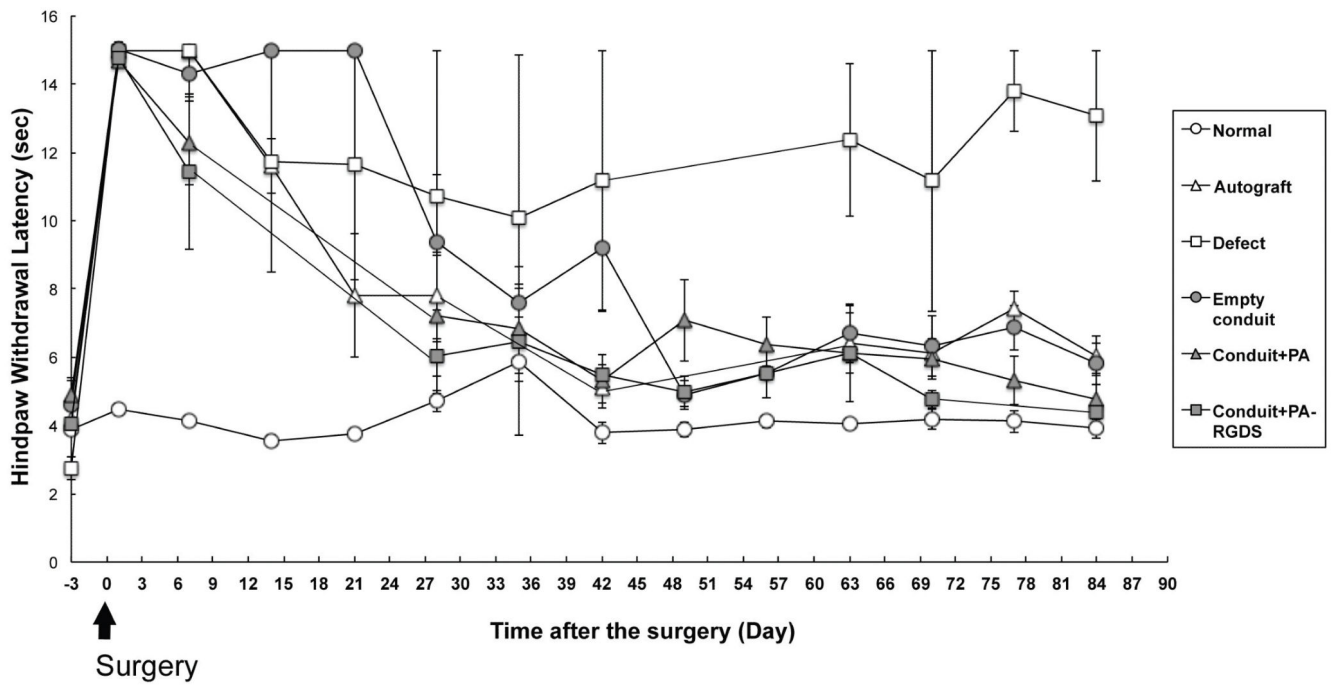
Fig. 7.
Hind paw latency to withdrawal in seconds plotted against postoperative day. Results from the various experimental conditions are presented.
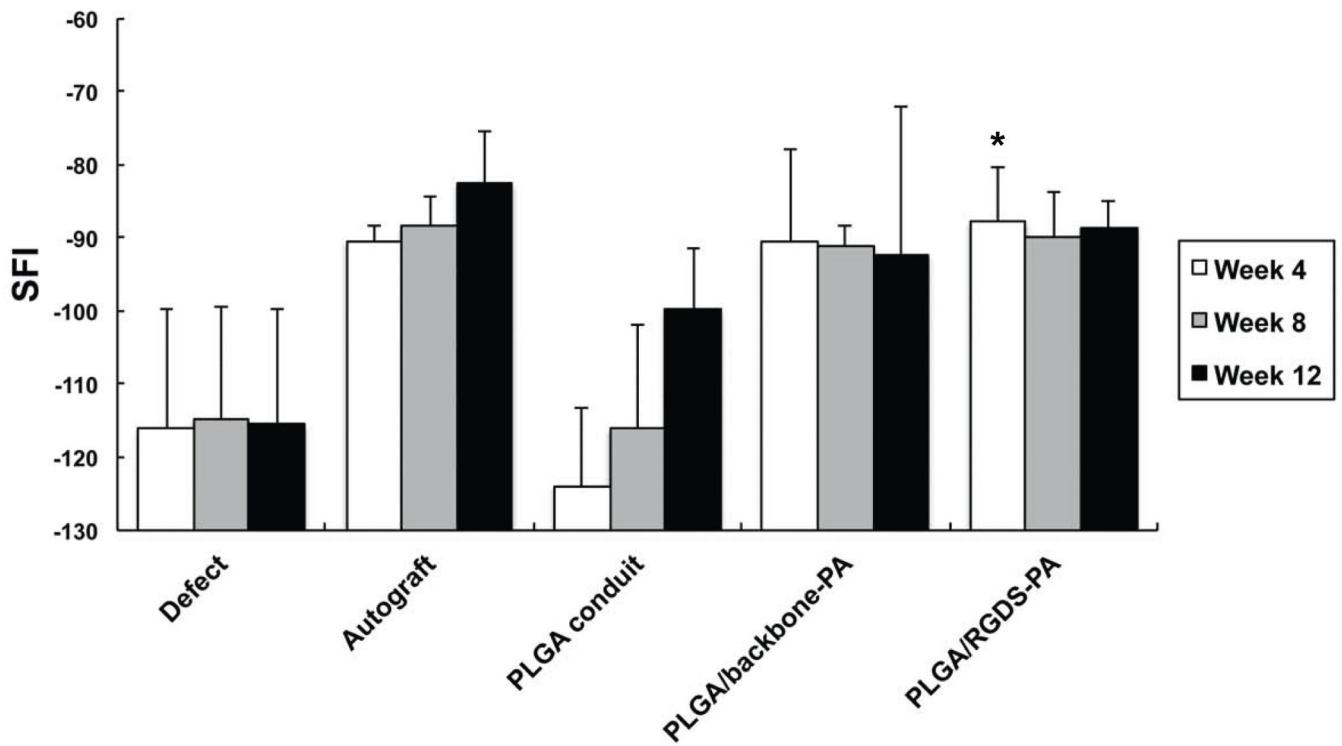
Fig. 8.
Gait was measured by examination of footprint patterns during ambulation at different time points (4, 8, and 12 weeks) following sciatic nerve transection. This data was used to calculate the SFI. * $p < 0.05$ vs. empty conduit at Week 4.
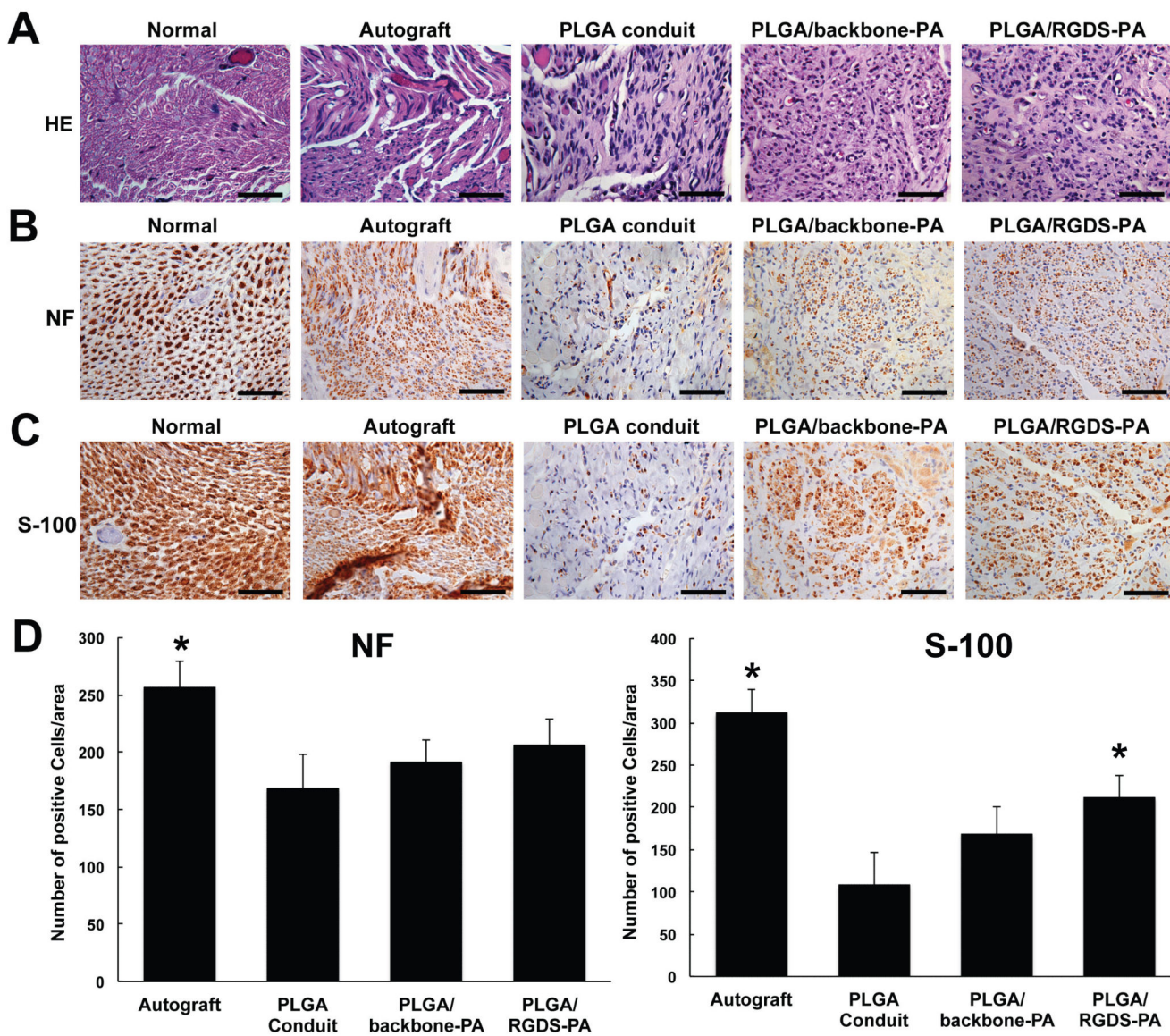
Fig. 9.
Histological findings at postoperative week 12. (**A**) The transverse sections of autograft, empty conduit, backbone-PA, and PLGA/RGDS-PA groups compared with that of normal sciatic nerve were analyzed by H.E. staining. (**B**) Immunohistochemistry staining with anti-neurofilament antibody (NF) in transverse sections of autograft, empty conduit, backbone-PA, and PLGA/RGDS-PA groups compared with that of normal control nerves. The nuclei were counterstained with hematoxylin. (**C**) Immunohistochemistry staining of the Schwann cell marker S-100 in transverse sections of autograft, empty conduit, backbone-PA, and PLGA/RGDS-PA groups compared with that of normal nerve. The nuclei were counterstained with hematoxylin. Bar=50 μm (D) The number of NF (left) and S-100 (right) positive cells of each groups. * $p<0.05$ vs. empty conduit.